Lattice Thermal Conductivity of Polyethylene Molecular Crystals from First-Principles Including Nuclear Quantum Effects

Nina Shulumba, Olle Hellman, and Austin J. Minnich[*]

Division of Engineering and Applied Science, California Institute of Technology, Pasadena, California 91125, USA

Molecular crystals such as polyethylene are of intense interest as flexible thermal conductors, yet their intrinsic upper limits of thermal conductivity remain unknown. Here, we report a study of the vibrational properties and lattice thermal conductivity of a polyethylene molecular crystal using an *ab initio* approach that rigorously incorporates nuclear quantum motion and finite temperature effects. We obtain a thermal conductivity along the chain direction of around 160 W m^{-1} K^{-1} at room temperature, providing a firm upper bound for the thermal conductivity of this molecular crystal. Furthermore, we show that the inclusion of quantum nuclear effects significantly impacts the thermal conductivity by altering the phase space for three-phonon scattering. Our computational approach paves the way for *ab initio* studies and computational material discovery of molecular solids free of any adjustable parameters.

Polymers have long been of interest for their potential as flexible thermal conductors in applications such as flexible electronics [1–4]. In bulk form, essentially all polymers are thermal insulators, with a thermal conductivity of less than 1 W m^{-1} K^{-1}, due to the random orientation of the molecular chains [5]. However, samples with highly aligned molecular chains may exhibit thermal conductivities as much as 2 orders of magnitude larger. Early work by Choy, Chen, and Luk [6] demonstrated that increasing the crystallinity in polymers drives an increase in thermal conductivity along the direction of the covalently bonded molecular chains. In low-density polyethylene, for instance, they reported increased thermal conductivity along the chain direction from 0.4 to 1.5 W m^{-1} K^{-1} when the polymers are stretched by a factor of 5. Other experiments on mechanically stretched bulk polyethylene [7,8] report thermal conductivities as high as ~42 W m^{-1} K^{-1} along the stretching direction due to crystalline alignment of the chains.

More recently, Shen *et al.* [9] reported a high thermal conductivity of around 100 W m^{-1} K^{-1} in high-quality ultradrawn polyethylene nanofibers. Wang *et al.* [10] used an optical method to study heat transport along polymer fibers, reporting thermal conductivity on the order of tens of W m^{-1} K^{-1} for polymers such as crystalline polyethylene and poly (*p*-phenylene benzobisoxazole). Singh *et al.* [11] reported amorphous aligned polythiophene fibers with a thermal conductivity of around 4 W m^{-1} K^{-1}, a factor of 20 increase over that of the unaligned fibers.

Despite these experimental advances, the theoretical treatment of heat transport in molecular crystals remains less developed. Molecular dynamics has been used in many studies to examine heat transport in polymers such as stretched polyethylene [12] and polydimethylsiloxane [13]. However, the semiempirical potentials used in these studies restrict their predictive power, especially for the polymers for which experimental data are scarce or unavailable.

Additionally, as with covalent crystals, semiempirical potentials are typically not designed to yield accurate cubic force constants, resulting in discrepancies in theoretical predictions of thermal conductivity for polymers. For instance, reports of thermal conductivity of polyethylene obtained by classical molecular dynamics with different potentials vary from ~45 [14] to 310 ± 190 W m^{-1} K^{-1} [15]. As a result, a rigorous upper bound for the thermal conductivity of molecular crystals such as polyethylene is lacking.

In addition to this challenge, most prior molecular dynamics simulations use a finite temperature description based on classical statistics of the nuclei motion [9,11]. This assumption is valid as long as zero-point motion can be neglected. However, molecular crystals like polyethylene contain large numbers of hydrogen atoms which have zero-point kinetic energy corresponding to around 1000 K. Excluding nuclear quantum effects leads to serious errors in other calculations, for instance, incorrectly predicting the phase stability of crystalline hydrogen [16,17] and structural and electronic fluctuations in water [18–20]. However, the impact of nuclear quantum effects on thermal transport properties has been minimally studied and cannot be accounted for with typical finite-displacement methods used for covalent crystals.

In this Letter, we investigate the lattice dynamics and the intrinsic thermal conductivity of crystalline polyethylene using an *ab initio* approach that rigorously includes nuclear quantum motion and finite temperature effects. We obtain a thermal conductivity of 164 W m^{-1} K^{-1} at room temperature, providing a rigorous upper bound for the intrinsic thermal conductivity of crystalline polyethylene. We also find that nuclear quantum motion has an unexpectedly large impact on the thermal conductivity by altering the phonon dispersion and thereby modifying the phonon scattering phase space compared to the classical prediction. Our computational approach paves the way for *ab initio* studies and computational material discovery of molecular solids without any adjustable parameters.

We study thermal conduction in crystalline polyethylene by lattice vibrations using the density functional theory in the Born-Oppenheimer approximation. We use the temperature-dependent effective potential method (TDEP) [21–23] to account for the zero-point motion and the thermal fluctuations of the nuclei following Bose-Einstein statistics. TDEP has been extensively described in prior publications. Briefly, the method identifies effective harmonic and cubic interatomic force constants consistent with the thermal displacements and forces of a canonical ensemble at a specified temperature. These force constants represent the best possible representation of the Born-Oppenheimer potential energy surface for atomic displacements around the equilibrium positions. These force constants can then be used in conjunction with the anharmonic perturbation theory to calculate lattice dynamics and thermal conductivity [24].

In prior implementations of TDEP, forces and displacements were obtained by performing *ab initio* molecular dynamics with a canonical ensemble. Recently, we reported an efficient stochastic method for TDEP that eliminates the need to perform *ab initio* molecular dynamics [25]. Briefly, we use the eigenvectors of the crystal structure to generate snapshots of the supercell with thermal displacements corresponding to a specified temperature rather than using molecular dynamics with a thermostat. To begin the procedure, we obtain the normal modes of the crystal using a model potential and generate the snapshots with thermal displacements for canonical ensembles at temperature T according to the desired thermal occupation function. We then evaluate interatomic forces for each snapshot using a standard quantum mechanical code. TDEP iteratively generates new force constants from forces and displacements and new snapshots from force constants until achieving self-consistency. Further details are available in Ref. [25]. The snapshot technique with classical occupation statistics has previously been used by West and Estreicher [26] and Souvatzis *et al.* [27], with quantum statistics by Errea, Calandra, and Mauri [28], among others and has a long history [29].

Accounting for Bose-Einstein statistics, and particularly zero-point motion, is especially important in molecular crystals due to the presence of many H atoms, yet most prior thermal conductivity calculations assumed Maxwell-Boltzmann (classical) statistics and ignored these effects. In this work, we account for nuclear quantum effects of the atoms in the ensemble using thermal amplitudes given by the Bose-Einstein distribution rather than classical statistics. Specifically, the thermal amplitudes are given by

$$\langle A_{is} \rangle = \underbrace{\sqrt{\frac{\hbar(2n_s + 1)}{2m_i\omega_s}}}_{\text{quantum}} \approx \underbrace{\frac{1}{\omega_s}\sqrt{\frac{k_B T}{m_i}}}_{\text{classical}}. \quad (1)$$

Here A_{is} is the amplitude of mode s projected onto atom i with mass m_i, ω_s is the normal mode frequency, and n_s is the thermal occupation factor. In this way, a simple modification to the method of Ref. [25] enables nuclear

quantum effects to be rigorously incorporated into the calculation with no additional computational expense.

Forces are calculated via the projector augmented wave method [30], as implemented in VASP [31–34]. In this work, the procedure to obtain self-consistent force constants required eight iterations, where calculating normal modes, generating snapshots, calculating forces, and fitting force constants define an iteration. Each iteration used 600 snapshots to ensure sufficient constraints to the IFCs and their convergence within each iteration. Crystalline polyethylene was modeled as $5 \times 3 \times 2$ repetitions of the fully relaxed orthorhombic unit cell containing 12 atoms which belong to two chains of C_2H_4 molecules. The plane wave energy cutoff was set at 800 eV, and Brillouin zone integrations were carried out on a $3 \times 3 \times 3$ mesh.

Exchange-correlation and van der Waals interactions were treated with the van der Waals (vdW) density functional [35–37]. Recent works have reported advances in the treatment of vdW interactions. Brown-Altvater, Rangel, and Neaton [38] showed that including vdW interactions enabled the accurate prediction of structural parameters and phonon frequencies of crystalline naphthalene. Kleis *et al.* [39] accurately predicted structural, cohesive, and elastic properties for crystalline polyethylene by including vdW interactions via the vdW density functional [35]. In this work, we employ the vdW density functional, as it has no empirical input or fitted parameters, has been tested for the polyethylene crystal [39], and leads to a stable structure with correct values for the elastic constants as well as structural parameters such as lattice parameters and angular orientation of the polymer chains.

We performed calculations on a grid on five temperatures, $\{100, 150, 300, 450, 600\}$ K, and six volumes. For each volume, the structure was fully relaxed until forces on the atoms were less than 10^{-7} eV/Å. The harmonic and cubic interatomic force constants for temperatures and volumes between these grid points were obtained by interpolation. Using TDEP method, we obtained the Helmholtz free energy surface $F(V, T)$, minimized the free energy to calculate the equilibrium volume at each temperature, and evaluated vibrational and transport properties at these conditions.

The thermal conductivity is calculated by iteratively solving the full Boltzmann transport equation (BTE) [24] on a $45 \times 45 \times 45$ q-point grid on which momentum is exactly conserved. For energy conservation we employed the tetrahedron approach [40]. Isotopic scattering [41] from the natural distribution is included in the iterative solution of the BTE.

As an initial validation of our calculations, we compare the phonon spectral function along the chain direction with the available experimental measurements [42,43]. The result is shown in Fig. 1(c) along with the experimental data at 25 K. The calculated frequencies of longitudinal and transverse acoustic modes agree well with available experimental data.

We next proceed to compute the thermal conductivity of the polyethylene molecular crystal versus temperature. The result is shown in Fig. 2(a), demonstrating a thermal conductivity along the chain direction of around 160 W m^{-1} K^{-1} at room temperature and a weak temperature dependence.
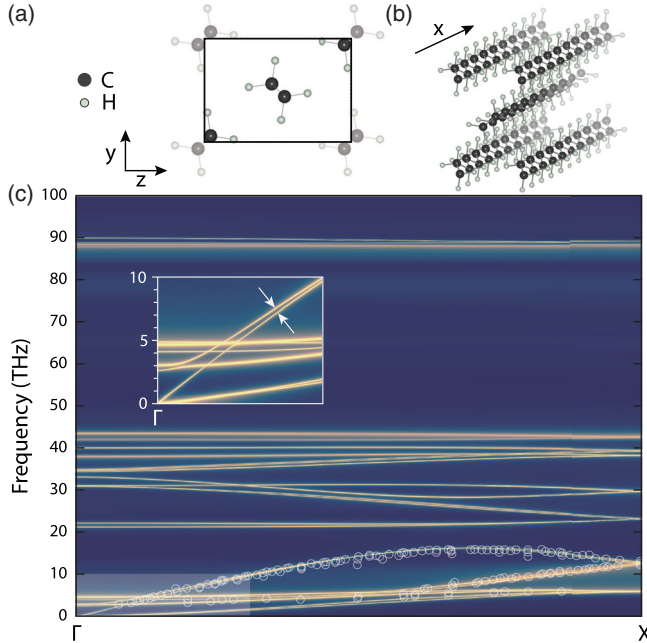
FIG. 1. (a) Enclosed in the box is a unit cell of bulk crystalline polyethylene, containing two molecular chains, projected onto the yz plane where the x coordinate is along the chain. (b) A 3D representation of the bulk crystalline polyethylene. The polyethylene crystal is formed from long parallel polymer chains and stabilizes in the base-centered orthorhombic crystal structure, confirmed by x-ray and neutron scattering measurements [44–46]. (c) Spectral function along the chain direction at 25 K compared with experimental data for the longitudinal [42] and transverse [43] acoustic modes. Inset: Longitudinal optical and acoustic modes are close in frequency above 5 THz.

The thermal conductivity perpendicular to the chain direction is around 2.5 W m^{-1} K^{-1}, demonstrating that the polyethylene crystal is highly thermally anisotropic. At 100 K, the thermal conductivity increases to around 300 W m^{-1} K^{-1} along the chain and 8 W m^{-1} K^{-1} in the normal directions. Our calculation, which included neither semiempirical potentials nor other fitting parameters, thus provides a rigorous upper bound for the intrinsic thermal conductivity of polyethylene crystals.

The obtained thermal conductivity is in reasonable agreement with prior experimental and computational works. Computationally, thermal conductivity for crystalline PE using classical MD simulations was predicted to range from ∼45 [14] to 310 ± 190 W m^{-1} K^{-1} [15]. Although these calculations used semiempirical potentials, their results are not expected to be orders of magnitude different than the actual value, and thus our calculated value is at least qualitatively consistent with these results.

Experimental reports of thermal conductivity of drawn polyethylene range from around 20–40 W m^{-1} K^{-1} [7,10] to around ∼100 W m^{-1} K^{-1} for a nanofiber [9]. Our work suggests that the thermal conductivity of the nanofiber nears the intrinsic thermal conductivity of polyethylene crystals. As experimental samples may contain various types of defects, we examine the influence of point defects
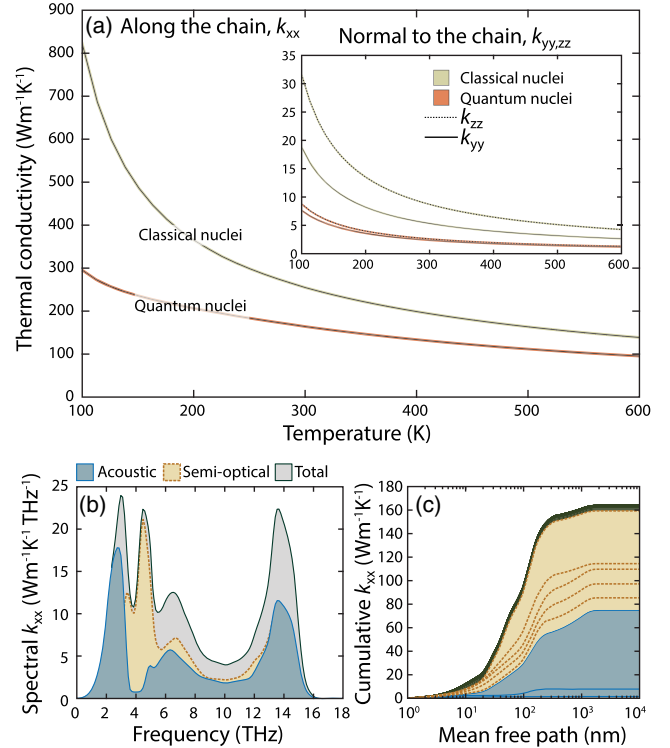

FIG. 2. (a) Calculated thermal conductivity of a polyethylene molecular crystal along the chain direction as a function of the temperature including nuclear quantum effects (red line) and assuming classical statistics (yellow line). Inset: Thermal conductivity, normal to the chain direction. (b) Total spectral thermal conductivity and spectral conductivity decomposed into acoustic and semioptical modes at room temperature. The contribution of the optical modes above 20 THz to the thermal conductivity is negligible. In the frequency region between 8 and 16 THz, the longitudinal acoustic and optical modes carry the most heat. (c) Cumulative thermal conductivity as a function of the mean free path. Most heat is conducted by longitudinal modes with comparable mean free paths that are less than 1 μm. The mean free paths of semioptical and transverse acoustic modes do not exceed 100 nm.

on thermal conductivity by incorporating oxygen as point (mass) defects, substituted on C sites, using the Tamura formula [41]. With 0.25 at. % oxygen, thermal conductivity reduces by 28% to 118 W m^{-1} K^{-1}, indicating that the thermal conductivity is sensitive to this type of defect.

For comparison, additional calculations were performed using classical statistics in which thermal displacements follow the Maxwell-Boltzmann distribution rather than the Bose-Einstein distribution. Interestingly, the thermal conductivity along the PE chain using classical statistics is considerably higher by around 50% at room temperature and more than a factor of 2 larger at 100 K. It is important to note that the quantum and classical calculations differ by only the thermal displacements and, hence, the regions of phase space sampled to construct effective Hamiltonians.

We want to emphasize the importance of vdW interactions in the calculation. Although we found our calculation to be insensitive to the particular choice of vdW functional used,
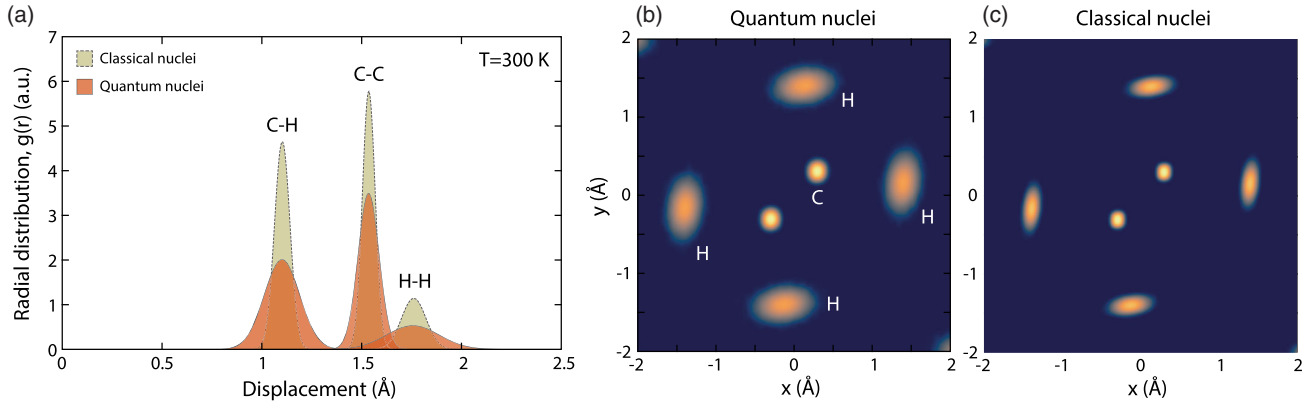
FIG. 3.   (a) Radial distribution function at room temperature. Atomic probability distribution (b) with and (c) without nuclear quantum effects. Zero-point motion increases the thermal displacements for all atoms but particularly for the hydrogen atoms.

including these weak interactions was essential, both to stabilize the structure and to account for additional interchain scattering processes. The absence of vdW interactions causes an underestimation of interchain scattering and a significant increase in thermal conductivity along the chain direction.

We provide additional insight into the thermal transport properties by calculating the spectral thermal conductivity versus phonon frequency in Fig. 2(b). We further decompose the total spectral conductivity at 300 K into the contributions of acoustic and semioptical modes. We define semioptical modes as nonacoustic modes below 20 THz, since contributions to the thermal conductivity from optical modes above 20 THz are negligible ($\sim 3\%$). Transverse modes [47] contribute to the total thermal conductivity significantly in the frequency region below 8 THz but make up only 20% of the overall value. Longitudinal modes carry the rest of the heat and equally contribute to heat conduction above 10 THz.

Although modes with frequencies exceeding 20 THz do not carry heat, they play an important role in thermal transport by acting as scattering channels for lower-frequency phonons, as previously reported for optic modes in Si [48]. Neglecting these modes leads to factor of 2 increases in thermal conductivity, demonstrating their importance to the phonon scattering phase space.

We also plot the cumulative thermal conductivity versus mean free path in Fig. 2(c). The figure shows that the contribution to the accumulation from the longitudinal acoustic and longitudinal optic modes is similar due to the near degeneracy of these modes. Around 60% of the heat is carried by vibrations with mean free paths under 100 nm and nearly all by mean free paths less than 1 μm. This mean free path distribution is quite different than that in silicon, in which 40% of the heat is carried by phonons with mean free paths exceeding 1 μm despite the two crystals possessing nearly the same thermal conductivity at room temperature.

We now examine the origin of the difference in thermal conductivity between the quantum and classical calculations. We first show the radial distribution function of the atoms in the ensemble at 300 K in Fig. 3(a). Unlike in covalent crystals with heavy atoms in which zero-point

motion is negligible, here quantum statistics leads to a far broader distribution of pair distances due to the zero-point motion. For vibrations involving C—C motions, the difference between classical and quantum thermal displacement magnitudes is only about 30%, but for C—H the thermal displacements including zero-point motion are around 60% larger and for H—H quantum statistics gives a distribution that is twice as wide as that of the classical calculation. Examining the cross section of probability densities perpendicular to the chain [Figs. 3(b) and 3(c)], we see that hydrogen experiences larger motions perpendicular to the bond direction than along it, indicating a weakening of bond-bending forces. The largest difference in the probability distribution between Maxwell-Boltzmann statistics and Bose-Einstein statistics exists in the direction of the C—H bond. Quantum statistics also affect the angular distribution of the bonds, for example, the H—C—H bond, but the effect is less pronounced than for the pair bonds.

To yield more insight into how these differences affect the thermal conductivity, we examine the phonon frequencies below 8 THz. In Figs. 4(a) and 4(b), we plot histograms of phonon frequencies as a function of the magnitude of the wave vector **q** with and without quantum effects. We
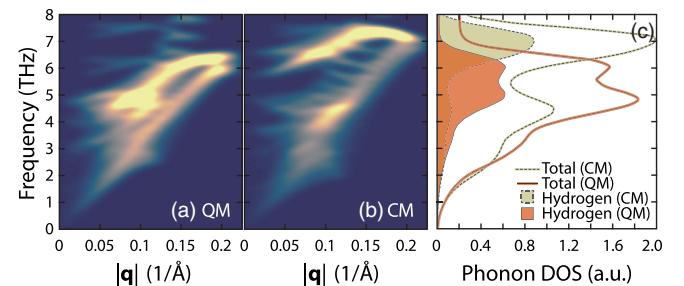

FIG. 4.   Spectral function versus wave vector magnitude **q** using (a) quantum mechanics and (b) classical statistics. (c) Total and site-projected phonon density of states. Filled regions correspond to the hydrogen contribution to the total density of states (solid and dashed lines). In the quantum case, hydrogen participates in 20% of the motions in the low-frequency region, while with classical statistics the fraction is less than 8%.

observe that the acoustic mode frequencies are qualitatively different when quantum effects are included. Specifically, the frequency gap between the transverse and longitudinal acoustic branches is smaller than in the classical case. As a result, for the quantum case, additional scattering channels exist compared to the classical case, leading to more scattering and lower thermal conductivity.

To demonstrate this point, we look at the species-projected phonon density of states in Fig. 4(c). Rather than being relegated to the high-frequency optical modes that contribute little to thermal transport, hydrogen participates in the motion of an unexpectedly large number of modes below 8 THz, where a large fraction of the heat is carried per Fig. 2(c). While classical statistics predicts that the hydrogen atoms participate in less than 8% of the total vibrational modes at frequencies below 8 THz, quantum statistics predicts a significantly larger contribution of 20%. A picture emerges where the large thermal displacements of hydrogen strongly affect the motions of carbon atoms, thereby altering the scattering phase space and reducing the thermal conductivity.

In summary, we present a study of the intrinsic lattice thermal conductivity for crystalline polyethylene using an *ab initio* approach that explicitly accounts for finite temperature and nuclear quantum effects. We obtain a thermal conductivity of $164 \ \mathrm{W\,m^{-1}\,K^{-1}}$ at room temperature, providing a rigorous upper bound for the intrinsic thermal conductivity of this molecular crystal. Furthermore, we show that nuclear quantum motion plays a significant role in setting the thermal conductivity by changing the frequencies of the low-frequency vibrations and, hence, the three-phonon scattering phase space. Our computational approach paves the way for *ab initio* studies and computational material discovery of molecular solids without any adjustable parameters.

---

*Corresponding author.
aminnich@caltech.edu

[1] S. R. Forrest, The path to ubiquitous and low-cost organic electronic appliances on plastic, Nature (London) **428,** 911 (2004).

[2] A. L. Moore and L. Shi, Emerging challenges and materials for thermal management of electronics, Mater. Today **17,** 163 (2014).

[3] H. Kang, S. Jung, S. Jeong, G. Kim, and K. Lee, Polymer-metal hybrid transparent electrodes for flexible electronics, Nat. Commun. **6,** 6503 (2015).

[4] Y. Wang, C. Zhu, R. Pfattner, H. Yan, L. Jin, S. Chen, F. Molina-Lopez, F. Lissel, J. Liu, N. I. Rabiah, Z. Chen, J. W. Chung, C. Linder, M. F. Toney, B. Murmann, and Z. Bao, A highly stretchable, transparent, and conductive polymer, Sci. Adv. **3,** e1602076 (2017).

[5] D. R. Anderson, Thermal conductivity of polymers, Chem. Rev. **66,** 677 (1966).

[6] C. L. Choy, F. C. Chen, and W. H. Luk, Thermal conductivity of oriented crystalline polymers, J. Polym. Sci. **18,** 1187 (1980).

[7] C. L. Choy, Y. W. Wong, G. W. Yang, and T. Kanamoto, Elastic modulus and thermal conductivity of ultradrawn polyethylene, J. Polym. Sci. **37,** 3359 (1999).

[8] D. B. Mergenthaler, M. Pietralla, S. Roy, and H. G. Kilian, Thermal conductivity in ultraoriented polyethylene, Macro-molecules **25,** 3500 (1992).

[9] S. Shen, A. Henry, J. Tong, R. Zheng, and G. Chen, Polyethylene nanofibres with very high thermal conductivities, Nat. Nanotechnol. **5,** 251 (2010).

[10] X. Wang, V. Ho, R. A. Segalman, and D. G. Cahill, Thermal conductivity of high-modulus polymer fibers, Macromolecules **46,** 4937 (2013).

[11] V. Singh, T. L. Bougher, A. Weathers, Y. Cai, K. Bi, M. T. Pettes, S. A. McMenamin, W. Lv, D. P. Resler, T. R. Gattuso, D. H. Altman, K. H. Sandhage, L. Shi, A. Henry, and B. A. Cola, High thermal conductivity of chain-oriented amorphous polythiophene, Nat. Nanotechnol. **9,** 384 (2014).

[12] J. Liu and R. Yang, Tuning the thermal conductivity of polymers with mechanical strains, Phys. Rev. B **81,** 174122 (2010).

[13] T. Luo, K. Esfarjani, J. Shiomi, A. Henry, and G. Chen, Molecular dynamics simulation of thermal energy transport in polydimethylsiloxane, J. Appl. Phys. **109,** 074321 (2011).

[14] A. Henry, G. Chen, S. J. Plimpton, and A. Thompson, 1D-to-3D transition of phonon heat conduction in polyethylene using molecular dynamics simulations, Phys. Rev. B **82,** 144308 (2010).

[15] B. Ni, T. Watanabe, and S. R. Phillpot, Thermal transport in polyethylene and at polyethylene-diamond interfaces investigated using molecular dynamics simulation, J. Phys. Condens. Matter **21,** 084219 (2009).

[16] N. D. Drummond, B. Monserrat, J. H. Lloyd-Williams, P. L. Ríos, Chris J. Pickard, and R. J. Needs, Quantum Monte Carlo study of the phase diagram of solid molecular hydrogen at extreme pressures, Nat. Commun. **6,** 7794 (2015).

[17] M. A. Morales, J. M. McMahon, C. Pierleoni, and D. M. Ceperley, Towards a predictive first-principles description of solid molecular hydrogen with density functional theory, Phys. Rev. B **87,** 184107 (2013).

[18] M. Ceriotti and D. E. Manolopoulos, Efficient First-Principles Calculation of the Quantum Kinetic Energy and Momentum Distribution of Nuclei, Phys. Rev. Lett. **109,** 100604 (2012).

[19] F. Giberti, A. A. Hassanali, M. Ceriotti, and M. Parrinello, The role of quantum effects on structural and electronic

fluctuations in neat and charged water, J. Phys. Chem. B **118**, 13226 (2014).

[20] M. Ceriotti, W. Fang, P. G. Kusalik, R. H. McKenzie, A. Michaelides, M. A. Morales, and T. E. Markland, Nuclear quantum effects in water and aqueous Systems: Experiment, theory, and current challenges, Chem. Rev. **116**, 7529 (2016).

[21] O. Hellman, I. A. Abrikosov, and S. I. Simak, Lattice dynamics of anharmonic solids from first principles, Phys. Rev. B **84**, 180301 (2011).

[22] O. Hellman, P. Steneteg, I. A. Abrikosov, and S. I. Simak, Temperature dependent effective potential method for accurate free energy calculations of solids, Phys. Rev. B **87**, 104111 (2013).

[23] O. Hellman and I. A. Abrikosov, Temperature-dependent effective third-order interatomic force constants from first principles, Phys. Rev. B **88**, 144301 (2013).

[24] D. A. Broido, M. Malorny, G. Birner, N. Mingo, and D. A. Stewart, Intrinsic lattice thermal conductivity of semiconductors from first principles, Appl. Phys. Lett. **91**, 231922 (2007).

[25] N. Shulumba, O. Hellman, and A. J. Minnich, Intrinsic localized mode and low thermal conductivity of PbSe, Phys. Rev. B **95**, 014302 (2017).

[26] D. West and S. K. Estreicher, First-Principles Calculations of Vibrational Lifetimes and Decay Channels: Hydrogen-Related Modes in Si, Phys. Rev. Lett. **96**, 115504 (2006).

[27] P. Souvatzis, O. Eriksson, M. I. Katsnelson, and S. P. Rudin, Entropy Driven Stabilization of Energetically Unstable Crystal Structures Explained from First Principles Theory, Phys. Rev. Lett. **100**, 095901 (2008).

[28] I. Errea, M. Calandra, and F. Mauri, Anharmonic free energies and phonon dispersions from the stochastic self-consistent harmonic approximation: Application to platinum and palladium hydrides, Phys. Rev. B **89**, 064302 (2014).

[29] M. L. Klein and G. K. Horton, The rise of self-consistent phonon theory, J. Low Temp. Phys. **9**, 151 (1972).

[30] P. E. Blöchl, Projector augmented-wave method, Phys. Rev. B **50**, 17953 (1994).

[31] G. Kresse and J. Hafner, *Ab initio* molecular dynamics for open-shell transition metals, Phys. Rev. B **48**, 13115 (1993).

[32] G. Kresse and J. Furthmüller, Efficient iterative schemes for *ab initio* total-energy calculations using a plane-wave basis set, Phys. Rev. B **54**, 11169 (1996).

[33] G. Kresse and J. Furthmüller, Efficiency of ab-initio total energy calculations for metals and semiconductors using a plane-wave basis set, Comput. Mater. Sci. **6**, 15 (1996).

[34] G. Kresse and D. Joubert, From ultrasoft pseudopotentials to the projector augmented-wave method, Phys. Rev. B **59**, 1758 (1999).

[35] M. Dion, H. Rydberg, E. Schröder, D. C. Langreth, and B. I. Lundqvist, van der Waals Density Functional for General Geometries, Phys. Rev. Lett. **92**, 246401 (2004).

[36] J. Klimeš, D. R. Bowler, and A. Michaelides, van der Waals density functionals applied to solids, Phys. Rev. B **83**, 195131 (2011).

[37] G. Román-Pérez and J. M. Soler, Efficient Implementation of a van der Waals Density Functional: Application to Double-Wall Carbon Nanotubes, Phys. Rev. Lett. **103**, 096102 (2009).

[38] F. Brown-Altvater, T. Rangel, and J. B. Neaton, *Ab initio* phonon dispersion in crystalline naphthalene using van der Waals density functionals, Phys. Rev. B **93**, 195206 (2016).

[39] J. Kleis, B. I. Lundqvist, D. C. Langreth, and E. Schröder, Towards a working density-functional theory for polymers: First-principles determination of the polyethylene crystal structure, Phys. Rev. B **76**, 100201 (2007).

[40] G. Lehmann and M. Taut, On the numerical calculation of the density of states and related properties, Phys. Status Solidi B **54**, 469 (1972).

[41] S.-i. Tamura, Isotope scattering of dispersive phonons in Ge, Phys. Rev. B **27**, 858 (1983).

[42] D. A. Braden, S. F. Parker, J. Tomkinson, and B. S. Hudson, Inelastic neutron scattering spectra of the longitudinal acoustic modes of the normal alkanes from pentane to pentacosane, J. Chem. Phys. **111**, 429 (1999).

[43] J. Tomkinson, S. F. Parker, D. A. Braden, and B. S. Hudson, Inelastic neutron scattering spectra of the transverse acoustic modes of the normal alkanes, Phys. Chem. Chem. Phys. **4**, 716 (2002).

[44] C. W. Bunn, The crystal structure of long-chain normal paraffin hydrocarbons. The "shape" of the CH2 group, Trans. Faraday Soc. **35**, 482 (1939).

[45] S. Kavesh and J. M. Schultz, Lamellar and interlamellar structure in melt-crystallized polyethylene. I. Degree of crystallinity, atomic positions, particle size, and lattice disorder of the first and second kinds, J. Polym. Sci. A **8**, 243 (1970).

[46] G. Avitabile, R. Napolitano, B. Pirozzi, K. D. Rouse, M. W. Thomas, and B. T. M. Willis, Low temperature crystal structure of polyethylene: Results from a neutron diffraction study and from potential energy calculations, J. Polym. Sci. C Polym. Lett. **13**, 351 (1975).

[47] N. Karasawa, S. Dasgupta, and W. A. Goddard, Mechanical properties and force field parameters for polyethylene crystal, J. Phys. Chem. **95**, 2260 (1991).

[48] A. Ward and D. A. Broido, Intrinsic phonon relaxation times from first-principles studies of the thermal conductivities of Si and Ge, Phys. Rev. B **81**, 085205 (2010).